Machine-Learning-Augmented Chemisorption Model for CO 2 Electroreduction Catalyst Screening

ARTICLE *in* JOURNAL OF PHYSICAL CHEMISTRY LETTERS · AUGUST 2015

Impact Factor: 7.46 · DOI: 10.1021/acs.jpclett.5b01660

Luke Achenie

Virginia Polytechnic Institute and State Univer…

The Journal of Physical Chemistry Letters

Letter

pubs.acs.org/JPCL

Machine-Learning-Augmented Chemisorption Model for CO_2 Electroreduction Catalyst Screening

Xianfeng Ma, Zheng Li, Luke E. K. Achenie, and Hongliang Xin*

Department of Chemical Engineering, Virginia Polytechnic Institute and State University, Blacksburg, Virginia 24061, United States

S *Supporting Information*

ABSTRACT: We present a machine-learning-augmented chemisorption model that enables fast and accurate prediction of the surface reactivity of metal alloys within a broad chemical space. Specifically, we show that artificial neural networks, a family of biologically inspired learning algorithms, trained with a set of *ab initio* adsorption energies and electronic fingerprints of idealized bimetallic surfaces, can capture complex, nonlinear interactions of adsorbates (e.g., *CO) on multimetallics with ~0.1 eV error, outperforming the two-level interaction model in prediction. By leveraging scaling relations between adsorption energies of similar adsorbates, we illustrate that this integrated approach greatly facilitates high-throughput catalyst screening and, as a specific case, suggests promising {100}-terminated multimetallic alloys with improved efficiency and selectivity for CO_2 electrochemical reduction to C_2 species. Statistical analysis of the network response to perturbations of input features underpins our fundamental understanding of chemical bonding on metal surfaces.

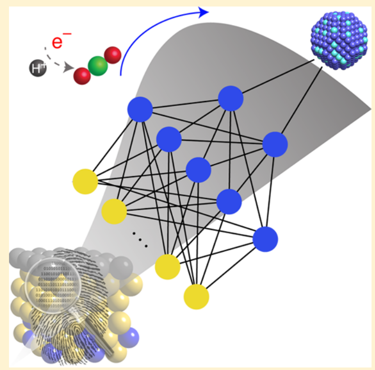

Bimetallic or multimetallic materials with atomically precise structure and composition have shown great promise for catalyzing many chemical and electrochemical reactions.[1−7] By exploiting the synergy of metallic species alloyed, surface sites with novel physicochemical properties can be realized. However, it is very time-consuming and costly to search for highly optimized alloys by high-throughput experiments and/or quantum-chemical calculations. In this regard, the *d*-band theory of chemisorption[8,9] that relates electronic properties of an active site to adsorption energies of critical surface intermediates (often termed as descriptors) provides physical insights into the characteristics of optimal catalysts and offers a theoretical basis for catalyst screening.[10−12] Due to the tight-binding approximation[13] employed in the *d*-band theory, only a subset of alloy materials that have relatively small perturbations to host metals can be directly explored at a reasonable accuracy,[10] which significantly limits its application. Herein we tackle this problem by developing a machine-learning-augmented chemisorption model that captures complex, nonlinear adsorbate−substrate interactions through artificial neural networks (ANNs) and thus enables large-scale exploration of reactivity descriptors in alloy materials space.

In this work, electrochemical reduction of carbon dioxide (CO_2) on metal electrodes is used as an example because of current interest in this process for sustainable production of fuels and value-added chemicals.[14−18] Among transition and post-transition metals, copper (Cu) shows pronounced activities for CO_2 electroreduction attributed to its balanced surface reactivity, i.e., adsorbing CO_2 and surface intermediates strongly to break required chemical bonds but weakly enough that those species can be further reduced to hydrocarbons or oxygenates.[19,20] This reaction is known to be sensitive to the geometric arrangement of surface metal atoms.[21−26] For example, Cu(111) can reduce CO_2 to methane (CH_4) with ~50% Faradaic efficiency, albeit requiring very high overpotentials (~1.0 V).[17] Interestingly, Cu(100) is particularly selective to C_2 species, e.g., ethylene (C_2H_4) and ethanol (C_2H_5OH), at somewhat lower overpotentials (~0.8 V).[21,23,24,26] While controlling the shape of Cu nanoparticles with {100} surface terminations proves to be fruitful for CO_2 electroreduction,[26] further improvements in energy and atom efficiency to valuable C_2 species by designing {100}-terminated bimetallic or multimetallic materials are needed for global implementation of this technology.

Some recent studies on CO/CO_2 electroreduction over Cu(100) suggest that the dimerization of *CO with sequential electron and proton transfers governs onset potentials in C_2 pathways, while a concerted proton−electron transfer to *CO is the critical step in C_1 pathways.[16,22,27,28] Based upon this mechanism, we aim to identify reactivity descriptors that characterize efficient alloy electrocatalysts for selectively converting CO_2 to C_2 species. To properly describe relative energetics of competing C_1 and C_2 pathways on Cu(100), it is important to explicitly consider realistic electrochemical CO_2 reduction conditions under which a high coverage of *CO is observed.[29] Figure 1 shows the free energy of relevant steps along C_1 and C_2 pathways calculated using density functional theory (DFT) at 0 V and −0.7 V relative to the reversible hydrogen electrode (RHE), with 3/8 ML *CO. The free energy pathways calculated from the model with 1/8 ML *CO are provided in Supporting Information Figure S1 for

Received: July 31, 2015
Accepted: August 25, 2015
Published: August 25, 2015

DOI: 10.1021/acs.jpclett.5b01660
J. Phys. Chem. Lett. 2015, 6, 3528−3533

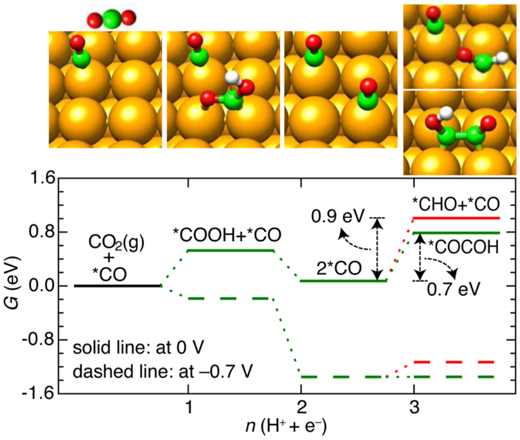

Figure 1. Most favorable free energy pathways to C_1 and C_2 species for CO_2 electroreduction on Cu(100) at 0 V and −0.7 V vs RHE, with snapshots of geometric structures of intermediates shown at the top. Note that only part of the surface model is shown for simplicity, and a more detailed picture of reaction intermediates can be found in Figure S2.

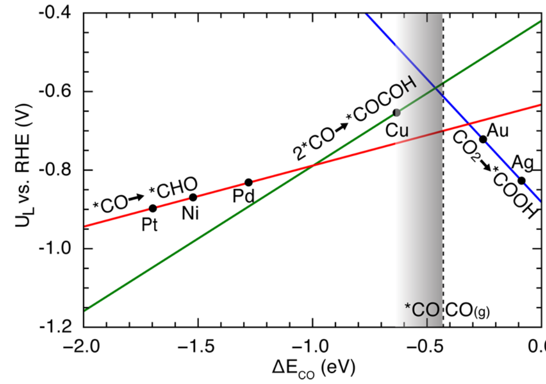

Figure 2. Predicted limiting potentials for key elementary steps of CO_2 electroreduction to C_1 and C_2 species as a function of CO adsorption energy at 1/8 ML. A few *d*-block transition metals are overlaid on the map. The CO desorption line is positioned where the elementary reaction CO(g) + * → *CO (low coverage limit) is in equilibrium at 0.01 atm partial pressure and 298.15 K (see Supporting Information for details).

comparison. Quantum ESPRESSO,[30] an open-source electronic structure code with plane-wave basis sets and ultrasoft pseudopotentials, is used for all the calculations shown here. The computational hydrogen electrode (CHE) model[31] is applied to account for electrode potentials in computing the free energy of a proton−electron pair ($H^+ + e^-$). Details of computational methods are shown in the Supporting Information, and energy corrections (electronic energy of gas phase molecules, zero-point energy, entropy, and solvation) can be found in Tables S1 and S2. Starting with 3/8 ML *CO that corresponds to a well-characterized $c(2 \times 2)$ surface structure[32] with 1/8 ML *CO vacancies, the protonation of *CO to *CHO is potential limiting in C_1 pathways with a −0.9 V_{RHE} theoretical onset potential, defined as the minimal applied electrode potential at which the free energy of a reaction pathway goes exergonic in all steps. By contrast, the formation of *COCOH from two adjacent *CO and a proton−electron pair has less negative onset potential (−0.7 V_{RHE}) in C_2 pathways. Considering the simplicity of such a model system without explicit inclusion of electric fields[28] and kinetic barriers,[28,33−35] the agreement between calculated onset potentials of C_1/C_2 pathways and recent experimental measurements of CO_2 electroreduction on Cu single crystals is remarkable.[26] The inability of the low-coverage model (1/8 ML *CO) in capturing the reactivity trends, as shown in Figure S1, emphasizes the critical role of adsorbate−adsorbate interactions in modulating energetics of surface reactions.

Using linear scaling relations[36] between adsorption energies of reaction intermediates on *CO precovered surfaces and the adsorption energy of *CO (ΔE_{CO}) at 1/8 ML (see Figure S3), we calculate the theoretical limiting potentials for key elementary steps in CO_2 electroreduction along C_1 and C_2 pathways as a function of the reactivity descriptor, i.e., the CO adsorption energy, shown in Figure 2. We note that the predicted CO adsorption energy (−0.63 eV) on Cu(100) at 1/8 ML using the Perdew−Burke−Ernzerhof (PBE) exchange-correlation functional agrees very well with the measured value (−0.66 eV) derived from the differential heat of chemisorption measurement from 0 to 1/8 ML *CO.[32,37] Volcano-like reactivity curves for C_1 and C_2 pathways are observed, where Cu is found to be close to the top, justifying the experimental observation of superior activity of Cu among transition metals for CO_2 electroreduction.[17] Moving toward the left leg will increase the overpotential for both pathways, although slightly favoring C_1 species formation. Weakening the bonding strength of *CO on a surface results in a less negative limiting potential from two adjacent *CO to *COCOH while the thermodynamic driving force from *CO to *CHO varies slowly due to a similar bonding configuration of *CO and *CHO, thus potentially enhancing the selectivity toward C_2 products. If a surface (e.g., Au and Ag) is too inert, either the formation of *COOH from CO_2 becomes potential-limiting or *CO would rather desorb into the gas phase instead of being further reduced. The optimal catalysts should have desired CO adsorption energy in the shaded region, i.e., 0−0.2 eV weaker than that on Cu(100). The question still remains, how can we possibly explore the infinite chemical space for alloys with desired properties?

To address this challenge, there have been significant efforts in developing predictive models relating surface reactivity of a metal site to its electronic properties that can then be inferred from standard tables or databases.[10−12,38] In this regard, the *d*-band theory, originally developed by Hammer and Nørskov, has been widely used to understand variations in adsorption energies of various adsorbates on pristine transition metal surfaces and their alloys.[8,9,39−42] The *d*-band center, ϵ_d, i.e., the weighted average energy of electronic *d*-states projected onto a surface metal atom, is one of the most important parameters within this theoretical framework. If the *d*-band center shifts up in energy, the adsorbate-metal antibonding states will also shift up and results in less occupation of antibonding states and thus stronger bonding. This simple picture of chemical bonding at metal surfaces has been verified using spectroscopic techniques.[43] Many studies have shown that the *d*-band model predicts reasonably well for surface reactivity of transition metals and a small subset of alloy materials.[10,42,44]

Still in pursuit is to develop a comprehensive chemisorption model that describes reactivity of alloy surfaces within a broad chemical space. A justification for searching for improved models is illustrated in Figure 3a, which shows a large deviation (root-mean-square error (RMSE) ∼0.3 eV) of predicted CO adsorption energies by the state-of-the-art two-level interaction model[39] within the framework of the *d*-band theory compared

DOI: 10.1021/acs.jpclett.5b01660
J. Phys. Chem. Lett. 2015, 6, 3528−3533

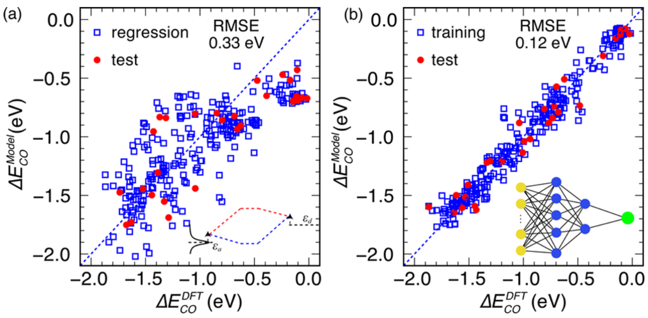

Figure 3. DFT-calculated CO adsorption energies on a set of idealized bimetallic surfaces versus prediction from (a) the two-level interaction model and (b) the machine-learning model. Insets show schematics of (a) the two-level interaction diagram and (b) the artificial neural network. Both reported RMSEs of the model prediction are the average over 16 repeated data randomization to avoid sampling bias.

to self-consistent DFT calculations for a set of {100}-terminated idealized bimetallic surfaces (see Figure S4 for structure details). In this model (see the Supporting Information for details), we have taken into account the hybridization of metal d-states with two renormalized resonance orbitals of *CO (5σ and $2\pi^*$), resulting from the embedding of gas phase molecular orbitals into a homogeneous electron gas. Energy levels of 5σ at −7.25 eV and $2\pi^*$ at 1.32 eV relative to the Fermi level are directly extracted from projected density of states of CO adsorbed on Al(100), which resembles the sp component of transition metal valence electrons. Ninety percent of ~250 bimetallic systems are randomly picked for a least squared regression of the interaction model using the DFT-calculated d-band center of clean surfaces and CO adsorption energies while the other 10% is used for prediction. The averaged RMSE of the model prediction with repeated random sampling is ~0.3 eV, larger than the desired energy window in Figure 2, which calls for a new model for catalyst screening purposes.

Motivated by ever-growing databases of materials properties, we use the machine-learning (ML) approach for mapping the problem of solving complex physical interactions to statistical models.[45−51] One of the most important ingredients for ML is the numerical representation of each learning example that reflects prior knowledge of the model for specific applications. Inspired by the d-band chemisorption theory, we use electronic properties of clean surfaces, namely, characteristics of the d-states distribution[13,41,42] including filling (zeroth moment up to the Fermi level), center (first moment relative to the Fermi level), width (square root of the second central moment), skewness (third standardized moment), and kurtosis (fourth standardized moment), together with the local Pauling electronegativity,[12] which is mainly determined by delocalized sp-states, as primary features. Host metal-dependent physical constants, such as spatial extent of metal d-orbitals,[13] adsorbate−metal interatomic d coupling matrix element squared, work function, atomic radius, ionization potential, electron affinity, and Pauling electronegativity as secondary features are also included for better description of trends of chemical bonding across a series of metal surfaces. All input features of alloy surfaces and corresponding CO adsorption energies are included in Table S3. Those properties form a unique fingerprint for each learning sample. Ideally, this vector can be estimated based on the tight-binding theory,[13] but in this work we obtain those properties as "byproducts" of the geometry optimization in DFT calculations.

Using a feedforward artificial neural network (ANN) model implemented in the open-source PyBrain code,[52] we attempt to construct a nonlinear mapping between the fingerprint vector in the preceding discussion and an output target function, i.e., CO adsorption energy. This algorithm has been successfully applied for materials properties predictions.[53−55] The network has a series of layers, and each layer consists of a number of neurons as processing units.[56] In a given layer, each neuron receives a set of weighted inputs from neurons of a previous layer and processes the cumulative input through an activation function (a sigmoid function for hidden layers and a linear function for the output layer) to produce an output. As the designated data set is processed through the network, the weights connecting different neurons are systematically adjusted using a gradient descent optimization algorithm until convergence. This initial process is the training of the network when the machine learns to make correct predictions on one set of data. Standardization of input features is performed for better performance of neural networks. During the training phase, a 10-fold cross validation with repeated randomization of data selection is used for determining the network structure (e.g., number of hidden layers and neurons within each hidden layer) and evaluating network performance. The above procedure is routinely applied in ANNs to avoid sampling bias and overly optimiztic error estimates. The network configuration of two hidden layers with 5 and 2 neurons, as illustrated in the inset of Figure 3b, gives the smallest prediction

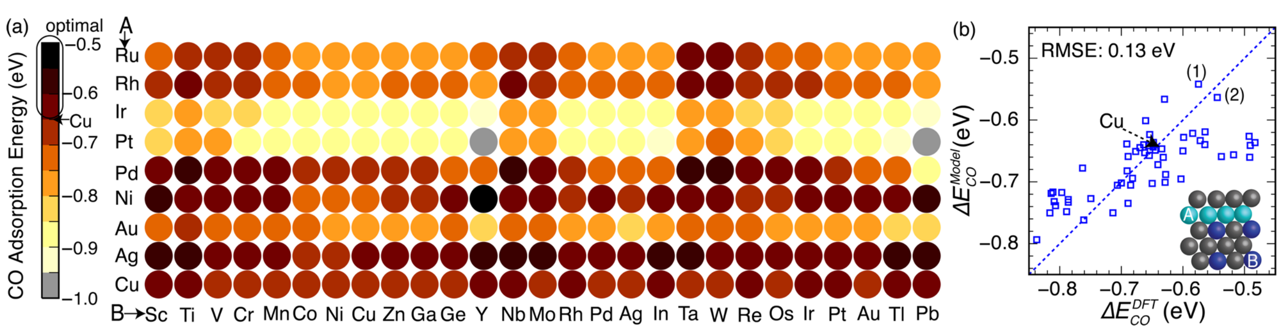

Figure 4. (a) Rational screening of CO adsorption energy on the second-generation core−shell alloy surfaces (Cu_3B-A@Cu_{ML}) using the developed neural-network model. (b) The parity plot shows a comparison of the CO adsorption energies on selected Cu monolayer alloys calculated using the neural-network model and self-consistent DFT. Two alloys, (1) Cu_3Y−Ni@Cu_{ML} and (2) Cu_3Sc−Ni@Cu_{ML}, are identified to have desired CO adsorption energies. The inset in panel b shows the geometric structure of the model system.

DOI: 10.1021/acs.jpclett.5b01660
J. Phys. Chem. Lett. 2015, 6, 3528−3533

error (~0.1 eV), which shows great promise compared to the two-level interaction model (~0.3 eV).

To assess the applicability of the model in practical catalyst design, we have used the neural-network model trained with all available data set of bimetallics for predicting CO adsorption energy on another type of Cu-based alloys (Cu_3B-A@Cu_{ML}) often termed as second-generation core−shell alloys, which has a monolayer of Cu metal atoms deposited on alloy surfaces with specific atomic ratios (e.g., Cu_3B) and one layer of another guest metal A as a buffer between them.[57] This type of alloy has shown great flexibility in design due to a potential utilization of both strain and ligand effects for tuning the reactivity of host metals,[58] and has been extensively studied for many electrochemical reactions, such as oxygen reduction in PEM fuel cells.[4−7,12] As shown in Figure 4a, many alloys are predicted to show desired CO binding energies, i.e., 0−0.2 eV weaker than CO adsorption on Cu(100). This task consumes a negligible CPU time using the neural-network model that would otherwise take weeks on hundreds of computers using standard DFT calculations. To further validate the model prediction, a subset of this type of alloy is calculated using DFT. Cu_3B−Ni@Cu_{ML} and Cu_3B−Rh@Cu_{ML} are selected for this purpose to have a large range of CO adsorption energies. Figure 4b shows that the neural-network predicted CO adsorption energy agrees very well with self-consistent DFT calculations (averaged RMSE 0.13 eV for 16 repeated random sampling in the network training).

To further shed light on underlying factors governing the adsorbate−substrate interactions, a sensitivity analysis of the derived neural network is performed using the "perturb" method.[59] The normalized sensitivity coefficient (NSC_i^M) for the input feature i and host metal M is calculated using

$$\mathrm{NSC}_i^M = \frac{1}{m}\sum_{j=1}^{m}\left|\frac{\partial \Delta E_j}{\partial z_j^i}\right| \cdot \frac{\max(z^i) - \min(z^i)}{\max(\Delta E) - \min(\Delta E)} \tag{1}$$

where z_j^i represents the input feature i of the sample j, which is perturbed up to +25%, ΔE_j is the CO adsorption energy of sample j, and m is the number of samples in the subset of M-based alloys. To allow direct comparison among inputs, an additional scaling factor is applied in eq 1 to normalize the output and also take into account the different scales of input features.[59] The *NSC* indicates the statistical importance of each feature in chemical bonding described by well-trained neural networks. The result is shown in Figure 5 for each primary feature i and host metal M. We can see that, (1) for all metal alloys the d-band center plays a relatively important role as suggested in the d-band theory; (2) the shape of the d-band characterized by higher moments of the d-states distribution has a higher significance for coinage metal alloys (Cu, Ag, and Au) than others (Ni, Pd, and Pt); and (3) the local Pauli electronegativity dictating the adsorbate-metal bonding distance and so interatomic coupling strength plays a much more important role in chemical bonding than we previously thought, and this is particularly the case for coinage metal alloys where the d-band is fully occupied and sp-band interactions dominate. This strongly suggests that the inclusion of d-band shape (higher moments of a d-band) and sp-band properties (local Pauli electronegativity) that are missing in the two-level interaction model is crucial for capturing the surface reactivity of transition metal alloys within a broad chemical space. The sensitivity analysis should not be used to undermine the importance of the d-band center in capturing trends of chemical bonding. We argue that the d-band center can be tuned easily through strain and ligand engineering, while other factors (e.g., the local Pauli electronegativity) vary slightly across the periodic table.

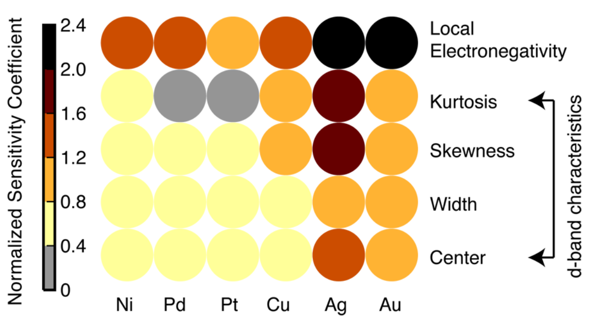

Figure 5. Normalized sensitivity coefficient obtained by analyzing the network response to perturbations of input features. The d-band filling is not analyzed here because it varies very little for a given type of alloys.

In conclusion, we have developed a machine-learning-augmented chemisorption model that captures complex, nonlinear adsorbate−substrate interactions using artificial neural networks and a set of ab initio calculations. With this model and the well-established descriptor-based catalyst design approach, we have identified promising {100}-terminated Cu multimetallics with a lower overpotential and possibly higher selectivity in CO_2 electoreduction to C_2 species. Statistical analysis of the network response to perturbations of input features underpins our understanding of chemical bonding on metal surfaces. The study opens a new way for designing metal-based catalysts with complexities, e.g., geometry and composition, promoters and poisons, defects, and nanoeffects.

■ ASSOCIATED CONTENT

Supporting Information

Details of computational methods, energy corrections, coverage effect, geometric structures, the description of the d-band model, and data used for machine learning. The Supporting Information is available free of charge on the ACS Publications website at DOI: 10.1021/acs.jpclett.5b01660.

(PDF)

■ AUTHOR INFORMATION

Corresponding Author

*E-mail: hxin@vt.edu.

Notes

The authors declare no competing financial interest.

■ ACKNOWLEDGMENTS

H.X. acknowledges the startup fund of Virginia Polytechnic Institute and State University. H.X. and X.M. give special thanks to Johannes Voss for developing the ase-espresso interface. This work is supported mainly by advanced research computing at Virginia Polytechnic Institute and State University and partially by the Extreme Science and Engineering Discovery Environment (XSEDE) through Grant No. DMR140106.

DOI: 10.1021/acs.jpclett.5b01660
J. Phys. Chem. Lett. 2015, 6, 3528−3533

REFERENCES

(1) Yu, W.; Porosoff, M. D.; Chen, J. G. Review of Pt-Based Bimetallic Catalysis: From Model Surfaces to Supported Catalysts. *Chem. Rev.* **2012**, *112*, 5780−5817.
(2) Rodriguez, J. Physical and Chemical Properties of Bimetallic Surfaces. *Surf. Sci. Rep.* **1996**, *24*, 223−287.
(3) Campbell, C. T. Bimetallic Surface Chemistry. *Annu. Rev. Phys. Chem.* **1990**, *41*, 775−837.
(4) Calle-Vallejo, F.; Koper, M. T. M.; Bandarenka, A. S. Tailoring the Catalytic Activity of Electrodes with Monolayer Amounts of Foreign Metals. *Chem. Soc. Rev.* **2013**, *42*, 5210−5230.
(5) Bandarenka, A. S.; Koper, M. T. M. Structural and Electronic Effects in Heterogeneous Electrocatalysis: Toward a Rational Design of Electrocatalysts. *J. Catal.* **2013**, *308*, 11−24.
(6) Nie, Y.; Li, L.; Wei, Z. Recent Advancements in Pt and Pt-free Catalysts for Oxygen Reduction Reaction. *Chem. Soc. Rev.* **2015**, *44*, 2168−2201.
(7) Wu, J.; Yang, H. Platinum-Based Oxygen Reduction Electrocatalysts. *Acc. Chem. Res.* **2013**, *46*, 1848−1857.
(8) Hammer, B.; Nørskov, J. K. Electronic Factors Determining the Reactivity of Metal Surfaces. *Surf. Sci.* **1995**, *343*, 211−220.
(9) Hammer, B.; Nørskov, J. K. Why Gold is the Noblest of All the Metals. *Nature* **1995**, *376*, 238−240.
(10) Xin, H.; Holewinski, A.; Schweitzer, N.; Nikolla, E.; Linic, S. Electronic Structure Engineering in Heterogeneous Catalysis: Identifying Novel Alloy Catalysts Based on Rapid Screening for Materials with Desired Electronic Properties. *Top. Catal.* **2012**, *55*, 376−390.
(11) İnoğlu, J. R.; Kitchin, N. Simple Model Explaining and Predicting Coverage-dependent Atomic Adsorption Energies on Transition Metal Surfaces. *Phys. Rev. B: Condens. Matter Mater. Phys.* **2010**, *82*, 045414.
(12) Xin, H.; Holewinski, A.; Linic, S. Predictive Structure Reactivity Models for Rapid Screening of Pt-Based Multimetallic Electrocatalysts for the Oxygen Reduction Reaction. *ACS Catal.* **2012**, *2*, 12−16.
(13) Harrison, W. A. *Electronic Structure and the Properties of Solids: The Physics of the Chemical Bond*; Dover Publications: Mineola, NY, 1989.
(14) Whipple, D. T.; Kenis, P. J. A. Prospects of CO_2 Utilization via Direct Heterogeneous Electrochemical Reduction. *J. Phys. Chem. Lett.* **2010**, *1*, 3451−3458.
(15) Costentin, C.; Robert, M.; Savéant, J.-M. Catalysis of the Electrochemical Reduction of Carbon Dioxide. *Chem. Soc. Rev.* **2013**, *42*, 2423−2436.
(16) Gattrell, M.; Gupta, N.; Co, A. A Review of the Aqueous Electrochemical Reduction of CO_2 to Hydrocarbons at Copper. *J. Electroanal. Chem.* **2006**, *594*, 1−19.
(17) Hori, Y. In *Modern Aspects of Electrochemistry*; Vayenas, C. G., White, R. E., Gamboa-Aldeco, M. E., Eds.; Modern Aspects of Electrochemistry 42; Springer: New York, 2008.
(18) Lu, Q.; Rosen, J.; Zhou, Y.; Hutchings, G. S.; Kimmel, Y. C.; Chen, J. G.; Jiao, F. A Selective and Efficient Electrocatalyst for Carbon Dioxide Reduction. *Nat. Commun.* **2014**, *5*, 3242.
(19) Peterson, A. A.; Nørskov, J. K. Activity Descriptors for CO_2 Electroreduction to Methane on Transition-Metal Catalysts. *J. Phys. Chem. Lett.* **2012**, *3*, 251−258.
(20) Peterson, A. A.; Abild-Pedersen, F.; Studt, F.; Rossmeisl, J.; Nørskov, J. K. How Copper Catalyzes the Electroreduction of Carbon Dioxide into Hydrocarbon Fuels. *Energy Environ. Sci.* **2010**, *3*, 1311−1315.
(21) Schouten, K. J. P.; Kwon, Y.; van der Ham, C. J. M.; Qin, Z.; Koper, M. T. M. A New Mechanism for the Selectivity to C_1 and C_2 Species in the Electrochemical Reduction of Carbon Dioxide on Copper Electrodes. *Chem. Sci.* **2011**, *2*, 1902−1909.
(22) Schouten, K. J. P.; Qin, Z.; Gallent, E. P.; Koper, M. T. M. Two Pathways for the Formation of Ethylene in CO Reduction on Single-Crystal Copper Electrodes. *J. Am. Chem. Soc.* **2012**, *134*, 9864−9867.
(23) Schouten, K. J. P.; Pérez Gallent, E.; Koper, M. T. M. Structure Sensitivity of the Electrochemical Reduction of Carbon Monoxide on Copper Single Crystals. *ACS Catal.* **2013**, *3*, 1292−1295.
(24) Hori, Y.; Takahashi, I.; Koga, O.; Hoshi, N. Electrochemical Reduction of Carbon Dioxide at Various Series of Copper Single Crystal Electrodes. *J. Mol. Catal. A: Chem.* **2003**, *199*, 39−47.
(25) Durand, W. J.; Peterson, A. A.; Studt, F.; Abild-Pedersen, F.; Nørskov, J. K. Structure Effects on the Energetics of the Electrochemical Reduction of CO_2 by Copper Surfaces. *Surf. Sci.* **2011**, *605*, 1354−1359.
(26) Roberts, F. S.; Kuhl, K. P.; Nilsson, A. High Selectivity for Ethylene from Carbon Dioxide Reduction over Copper Nanocube Electrocatalysts. *Angew. Chem.* **2015**, *127*, 5268−5271.
(27) Calle-Vallejo, F.; Koper, M. T. M. Theoretical Considerations on the Electroreduction of CO to C_2 Species on Cu(100) Electrodes. *Angew. Chem., Int. Ed.* **2013**, *52*, 7282−7285.
(28) Montoya, J. H.; Shi, C.; Chan, K.; Nørskov, J. K. Theoretical Insights into a CO Dimerization Mechanism in CO_2 Electroreduction. *J. Phys. Chem. Lett.* **2015**, *6*, 2032−2037.
(29) Hori, Y.; Koga, O.; Watanabe, Y.; Matsuo, T. FTIR Measurements of Charge Displacement Adsorption of CO on Poly- and Single Crystal (100) of Cu Electrodes. *Electrochim. Acta* **1998**, *44*, 1389−1395.
(30) Giannozzi, P.; Baroni, S.; Bonini, N.; Calandra, M.; Car, R.; Cavazzoni, C.; Ceresoli, D.; Chiarotti, G. L.; Cococcioni, M.; Dabo, I.; et al. QUANTUM ESPRESSO: A Modular and Open-source Software Project for Quantum Simulations of Materials. *J. Phys.: Condens. Matter* **2009**, *21*, 395502.
(31) Nørskov, J. K.; Rossmeisl, J.; Logadottir, A.; Lindqvist, L.; Kitchin, J. R.; Bligaard, T.; Jónsson, H. Origin of the Overpotential for Oxygen Reduction at a Fuel-Cell Cathode. *J. Phys. Chem. B* **2004**, *108*, 17886−17892.
(32) Tracy, J. C. Structural Influences on Adsorption Energy. II. CO on Ni(100). *J. Chem. Phys.* **1972**, *56*, 2736−2747.
(33) Montoya, J. H.; Peterson, A. A.; Nørskov, J. K. Insights into C−C Coupling in CO_2 Electroreduction on Copper Electrodes. *ChemCatChem* **2013**, *5*, 737−742.
(34) Nie, X.; Esopi, M. R.; Janik, M. J.; Asthagiri, A. Selectivity of CO_2 Reduction on Copper Electrodes: The Role of the Kinetics of Elementary Steps. *Angew. Chem., Int. Ed.* **2013**, *52*, 2459−2462.
(35) Nie, X.; Luo, W.; Janik, M. J.; Asthagiri, A. Reaction Mechanisms of CO_2 Electrochemical Reduction on Cu(111) Determined with Density Functional Theory. *J. Catal.* **2014**, *312*, 108−122.
(36) Abild-Pedersen, F.; Greeley, J.; Studt, F.; Rossmeisl, J.; Munter, T. R.; Moses, P. G.; Skulason, E.; Bligaard, T.; Norskov, J. K. Scaling Properties of Adsorption Energies for Hydrogen-Containing Molecules on Transition-Metal Surfaces. *Phys. Rev. Lett.* **2007**, *99*, 016105−4.
(37) Truong, C. M.; Rodriguez, J.; Goodman, D. W. CO Adsorption Isotherms on Cu(100) at Elevated Pressures and Temperatures Using Infrared Reflection Absorption Spectroscopy. *Surf. Sci.* **1992**, *271*, L385−L391.
(38) İnoğlu, N.; Kitchin, J. R. New Solid-state Table: Estimating *d*-band Characteristics for Transition Metal Atoms. *Mol. Simul.* **2010**, *36*, 633.
(39) Hammer, B.; Morikawa, Y.; Nørskov, J. K. CO Chemisorption at Metal Surfaces and Overlayers. *Phys. Rev. Lett.* **1996**, *76*, 2141.
(40) Xin, H.; Linic, S. Exceptions to the *d*-band Model of Chemisorption on Metal Surfaces: The Dominant Role of Repulsion Between Adsorbate States and Metal *d*-states. *J. Chem. Phys.* **2010**, *132*, 221101−221101−4.
(41) Xin, H.; Vojvodic, A.; Voss, J.; Nørskov, J. K.; Abild-Pedersen, F. Effects of *d*-band Shape on the Surface Reactivity of Transition-metal Alloys. *Phys. Rev. B: Condens. Matter Mater. Phys.* **2014**, *89*, 115114.
(42) Vojvodic, A.; Nørskov, J. K.; Abild-Pedersen, F. Electronic Structure Effects in Transition Metal Surface Chemistry. *Top. Catal.* **2014**, *57*, 25.

DOI: 10.1021/acs.jpclett.5b01660
J. Phys. Chem. Lett. 2015, 6, 3528−3533

(43) Pettersson, L. G. M.; Nilsson, A. A Molecular Perspective on the *d*-band Model: Synergy Between Experiment and Theory. *Top. Catal.* **2014**, *57*, 2−13.

(44) Nørskov, J. K.; Abild-Pedersen, F.; Studt, F.; Bligaard, T. Density Functional Theory in Surface Chemistry and Catalysis. *Proc. Natl. Acad. Sci. U. S. A.* **2011**, *108*, 937−943.

(45) Andriotis, A. N.; Mpourmpakis, G.; Broderick, S.; Rajan, K.; Datta, S.; Sunkara, M.; Menon, M. Informatics Guided Discovery of Surface Structure-chemistry Relationships in Catalytic Nanoparticles. *J. Chem. Phys.* **2014**, *140*, 094705.

(46) Rupp, M.; Tkatchenko, A.; Müller, K.-R.; von Lilienfeld, O. A. Fast and Accurate Modeling of Molecular Atomization Energies with Machine Learning. *Phys. Rev. Lett.* **2012**, *108*, 058301.

(47) Montavon, G.; Rupp, M.; Gobre, V.; Vazquez-Mayagoitia, A.; Hansen, K.; Tkatchenko, A.; Müller, K.-R.; von Lilienfeld, O. A. Machine Learning of Molecular Electronic Properties in Chemical Compound Space. *New J. Phys.* **2013**, *15*, 095003.

(48) Landrum, G. A.; Penzotti, J. E.; Putta, S. Machine-learning Models for Combinatorial Catalyst Discovery. *Meas. Sci. Technol.* **2005**, *16*, 270.

(49) Kusne, A. G.; Gao, T.; Mehta, A.; Ke, L.; Nguyen, M. C.; Ho, K.-M.; Antropov, V.; Wang, C.-Z.; Kramer, M. J.; Long, C. On-the-fly Machine-learning for High-throughput Experiments: Search for Rare-earth-free Permanent Magnets. *Sci. Rep.* **2014**, *4*, 6367.

(50) Hautier, G.; Fischer, C. C.; Jain, A.; Mueller, T.; Ceder, G. Finding Nature Missing Ternary Oxide Compounds Using Machine Learning and Density Functional Theory. *Chem. Mater.* **2010**, *22*, 3762−3767.

(51) Dam, H. C.; Pham, T. L.; Ho, T. B.; Nguyen, A. T.; Nguyen, V. C. Data Mining for Materials Design: A Computational Study of Single Molecule Magnet. *J. Chem. Phys.* **2014**, *140*, 044101.

(52) Schaul, T.; Bayer, J.; Wierstra, D.; Sun, Y.; Felder, M.; Sehnke, F.; Rückstieß, T.; Schmidhuber, J. PyBrain. *J. Mach. Learn. Res.* **2010**, *11*, 743−746.

(53) Scott, D. J.; Coveney, P. V.; Kilner, J. A.; Rossiny, J. C. H.; Alford, N. M. N. Prediction of the Functional Properties of Ceramic Materials from Composition Using Artificial Neural Networks. *J. Eur. Ceram. Soc.* **2007**, *27*, 4425−4435.

(54) Behler, J.; Parrinello, M. Generalized Neural-Network Representation of High-Dimensional Potential-Energy Surfaces. *Phys. Rev. Lett.* **2007**, *98*, 146401.

(55) Behler, J. Representing Potential Energy Surfaces by High-dimensional Neural Network Potentials. *J. Phys.: Condens. Matter* **2014**, *26*, 183001.

(56) Abu-Mostafa, Y. S.; Magdon-Ismail, M.; Lin, H.-T. *Learning From Data*; AMLBook.com, S.l., 2012.

(57) Gong, K.; Su, D.; Adzic, R. R. Platinum-Monolayer Shell on $AuNi_{0.5}Fe$ Nanoparticle Core Electrocatalyst with High Activity and Stability for the Oxygen Reduction Reaction. *J. Am. Chem. Soc.* **2010**, *132*, 14364−14366.

(58) Kitchin, J. R.; Nørskov, J. K.; Barteau, M. A.; Chen, J. G. Role of Strain and Ligand Effects in the Modification of the Electronic and Chemical Properties of Bimetallic Surfaces. *Phys. Rev. Lett.* **2004**, *93*, 156801.

(59) Engelbrecht, A. P.; Cloete, I.; Zurada, J. M. In *From Natural to Artificial Neural Computation*; Mira, J., Sandoval, F., Eds.; Lecture Notes in Computer Science 930; Springer: Berlin Heidelberg, 1995.

DOI: 10.1021/acs.jpclett.5b01660
J. Phys. Chem. Lett. 2015, 6, 3528−3533